Inorganic Chemistry

Article

pubs.acs.org/IC

Solid Solutions of Pauli-Paramagnetic $CaCu_3V_4O_{12}$ and Antiferromagnetic $CaMn_3V_4O_{12}$

Shoubao Zhang,[†] Takashi Saito,[†] Wei-Tin Chen,[†,‡] Masaichiro Mizumaki,[§] and Yuichi Shimakawa*[,†,⊥]

[†]Institute for Chemical Research, Kyoto University, Uji, Kyoto 611-0011, Japan

[§]Japan Synchrotron Radiation Research Institute, SPring-8, Sayo-gun, Hyogo 679-5198, Japan

[⊥]Japan Science and Technology Agency, CREST, Uji, Kyoto 611-0011, Japan

Supporting Information

ABSTRACT: Solid solutions of Pauli-paramagnetic $CaCu_3V_4O_{12}$ and antiferromagnetic $CaMn_3V_4O_{12}$ were prepared by a high-pressure synthesis technique. All samples crystallized in the A-site-ordered perovskite structure with isovalent Cu^{2+} and Mn^{2+} ions at the square-planar A′ site. The V ion at the B site kept a charge state close to +4 in all of the solid solutions, and the electrons of V were delocalized and contributed to the metallic properties. The substitution of Mn^{2+} for Cu^{2+} in $CaCu_3V_4O_{12}$, where both Cu and V electrons were delocalized, produced the $S = {}^5/_2$ localized moments, and the spins at the Mn site interacted antiferromagnetically. Spin-glass-like magnetic behaviors due to the random distribution of Cu/Mn ions at the A′ site were observed at intermediate compositions of the solid solution, whereas the antiferromagnetic transition was observed at the end composition $CaMn_3V_4O_{12}$.

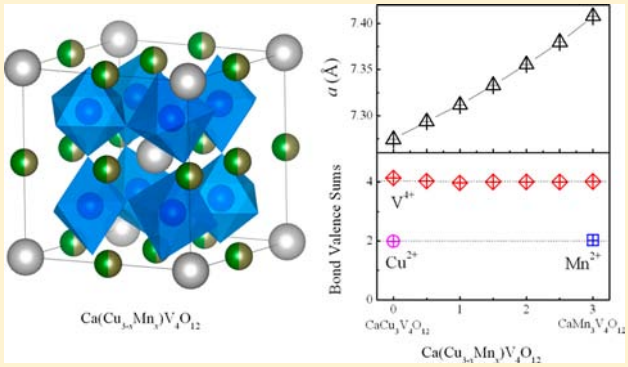

INTRODUCTION

A-site-ordered perovskite-structure oxides $AA'_3B_4O_{12}$, in which the A- and A′-site cations are ordered at an originally 12-fold-coordinated A site in a simple perovskite ABO_3, have been studied extensively because they show a wide variety of chemical and physical properties.[1−5] As shown in Figure 1, the A′ site in this structure is coordinated by four O atoms with short (~2.0 Å) bonds and by eight O atoms with relatively long (~2.6−3.2 Å) bonds and forms nearly square units that align perpendicular to each other. Cu and Mn ions are known to occupy such a square-coordinated A′ site, and Jahn−Teller distortions in Cu^{2+} and Mn^{3+} were thought to play important roles in stabilizing the ions at the site. $Ca^{2+}Cu^{2+}{}_3Ti^{4+}{}_4O_{12}$ and $Y^{3+}Mn^{3+}{}_3Al^{3+}{}_4O_{12}$ are typical examples of compounds in which those ions are stabilized at the A′ sites.[6,7]

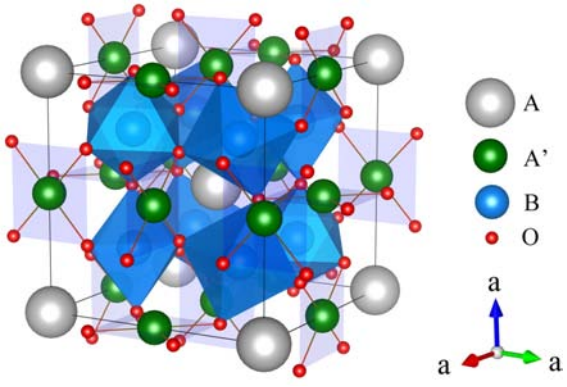

Figure 1. Crystal structure of the A-site-ordered perovskite $AA'_3B_4O_{12}$.

Recently, however, it was revealed that not only Jahn−Teller active Cu^{2+} and Mn^{3+} but also ions with other ionic states can be stabilized at the A′ sites in A-site-ordered perovskite-structure compounds. For example, an intersite charge transfer between the A′-site Cu and B-site Fe in $La^{3+}Cu^{2+}{}_3Fe^{3.75+}{}_4O_{12}$ stabilizes Cu^{3+} at the A′ site, producing $La^{3+}Cu^{3+}{}_3Fe^{3+}{}_4O_{12}$.[5] In $La_{1-x}Na_xMn_3Ti_4O_{12}$, substitution of Na^+ for some of La^{3+} ions changes the ionic state of Mn at the A′ site but not that of Ti^{4+} at the B site, resulting in compounds expressed nominally as $LaMn^{1.66+}{}_3Ti_4O_{12}$ ($x = 0.0$), $La_{0.5}Na_{0.5}Mn^{2+}{}_3Ti_4O_{12}$ ($x = 0.5$), and $NaMn^{2.33+}{}_3Ti_4O_{12}$ ($x = 1.0$).[8] Thus, not only Mn^{3+} but also Mn^{2+} and even Mn^+ can occupy the A′ site. This encouraged us to explore further possibilities for the isovalent substitution of Cu^{2+} for Mn^{2+} or Cu^{3+} for Mn^{3+}, and here we focus on solid solutions of $CaCu_3V_4O_{12}$ and $CaMn_3V_4O_{12}$ with the isovalent substitution of Cu^{2+} for Mn^{2+}.

The A-site-ordered perovskites with V at the B site show very interesting properties. Although $CaCu_3V_4O_{12}$ is considered to be an ionic crystal with an ionic formula of $Ca^{2+}Cu^{2+}{}_3V^{4+}{}_4O_{12}$, the compound shows a Pauli-paramagnetic and metallic behavior.[9] Both A′-site Cu and B-site V bands cross the Fermi level in the electronic structure, and electrons of both Cu and V are itinerant, leading to the metallic property. This

Received: June 27, 2013
Published: August 26, 2013

   dx.doi.org/10.1021/ic401633c | *Inorg. Chem.* 2013, 52, 10610−10614

itinerancy contrasts sharply with the localized electronic behaviors of Cu^{2+} at the A′ sites in many of the A-site-ordered perovskites. In the insulating $Ca^{2+}Cu^{2+}{}_3Ti^{4+}{}_4O_{12}$, indeed, Cu^{2+} ($S = {}^1/_2$) spins at the A′ site form a G-type antiferromagnetic spin structure.[4] On the other hand, $CaMn_3V_4O_{12}$ shows antiferromagnetism below 54 K.[10] Interestingly, the magnetism originates only from the Mn^{2+} ($S = {}^5/_2$) spins at the A′ site, while the electrons of B-site V appear to be delocalized and contribute to the low resistivity. No correlation was observed between the spins at A′-site Mn and the electrons at the B-site V.

In this study, we made solid solutions of the Pauli-paramagnetic $CaCu_3V_4O_{12}$ and antiferromagnetic-and-metallic $CaMn_3V_4O_{12}$. From analyses of the crystal and electronic structures and magnetic and electronic transport properties, we see how the properties of the solid solutions change.

EXPERIMENTAL SECTION

Samples with nominal compositions of $Ca(Cu_{3-x}Mn_x)V_4O_{12}$ (x = 0, 0.5, 1, 1.5, 2, 2.5, and 3) were prepared by solid-state reactions under high-temperature and high-pressure conditions. Stoichiometric amounts of the raw materials CaO, CuO, Mn_2O_3, V_2O_3, and V_2O_5 were mixed and sealed in gold capsules in a glovebox. They were then treated at 9 GPa and 900 °C for 30 min with a cubic-anvil-type high-pressure apparatus, followed by quenching to room temperature before the pressure was released.

Synchrotron powder X-ray diffraction (SXRD) patterns (wavelength λ = 0.775 Å) for phase identification and structural analysis were obtained at room temperature. Diffraction patterns were collected with a large Debye−Scherrer camera installed at BL19B2 in SPring-8, and the crystal structures were refined by the Rietveld method with the program *GSAS*.[11] The valence states of Mn, Cu, and V were investigated by X-ray absorption spectroscopy (XAS) measurements that were made at BL23SU in SPring-8 by a total electron yield method. The data were taken at 14 K, and the incident photon energy was calibrated by measuring the energies of the Ti $L_{3,2}$-edges of TiO_2 and the Ni $L_{3,2}$-edges of NiO.

Electronic resistivity measurements by a four-probe method were carried out in a Quantum Design Physical Property Measurement System, and the magnetic susceptibility in zero-field-cooled (ZFC) and field-cooled (FC) modes was measured in a Quantum Design Magnetic Property Measurement System with a reciprocating sample option.

The electronic structures of $CaCu_3V_4O_{12}$ and $CaMn_3V_4O_{12}$ were calculated by full-potential linearized augmented plane-wave (FLAPW) first-principle calculations with the *WIEN2k* code. The lattice parameters and fractional atomic positions experimentally obtained by the structure refinements were used for the calculations. The FLAPW sphere radii for Ca, Cu, Mn, V, and O were 2.0, 1.9, 1.9, 1.9, and 1.60 a.u., respectively. Self-consistency was carried out on 1000 k-point meshes in the whole Brillouin zone.

RESULTS AND DISCUSSION

Figure 2 shows the SXRD patterns of $Ca(Cu_{3-x}Mn_x)V_4O_{12}$ ($0 \le x \le 3$), and Figure 3 shows a typical result of the Rietveld structure refinements. The refined structural parameters and selected bond lengths and bond angles of all samples are listed in the Supporting Information. All samples were crystallized with the A-site-ordered perovskite structure with a cubic space group of $Im\bar{3}$, and although a very tiny amount of VO_2 was detected in the samples with $x > 0.5$, no significant impurity phases were observed. As is clearly seen in the enlarged view of the diffraction patterns around $2\theta = 53°$ in the inset, a peak shift to lower angles indicates a systematic increase in the lattice parameters with increasing Mn substitution. As shown in Figure 4a, the refined lattice parameters follow Vegard's law, indicating successful synthesis of the solid solutions.

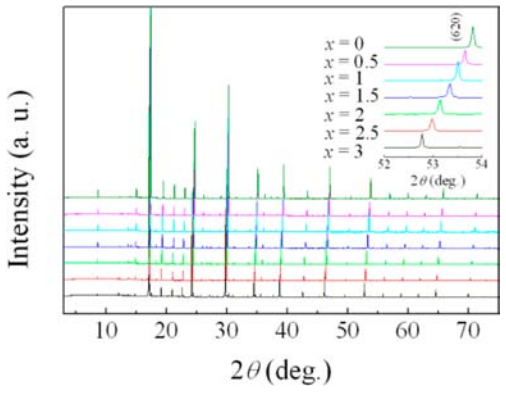

Figure 2. SXRD patterns of $Ca(Cu_{3-x}Mn_x)V_4O_{12}$ ($0 \le x \le 3$). The inset shows an enlarged view of the diffraction patterns around 2θ = 53°.

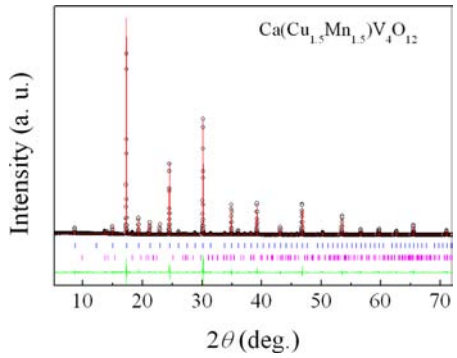

Figure 3. SXRD pattern and the result of Rietveld refinement for $Ca(Cu_{1.5}Mn_{1.5})V_4O_{12}$. The observed (circles), calculated (line), and difference (bottom line) patterns are shown. The ticks indicate the positions of the Bragg reflections. The small amount of the VO_2 impurity phase was included in the refinement. (Bragg reflection positions for VO_2 are indicated by the second low ticks.)

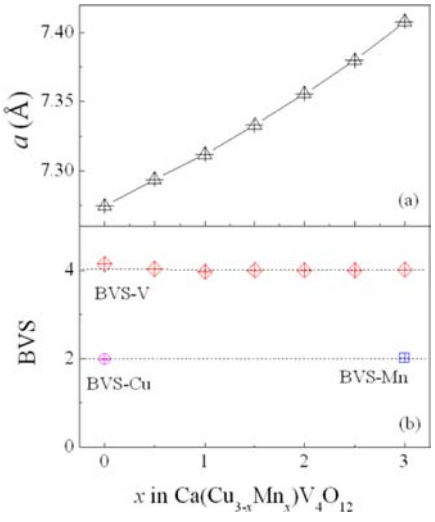

Figure 4. Changes in (a) the lattice parameter and (b) the BVS value for V in solid solution $Ca(Cu_{3-x}Mn_x)V_4O_{12}$ ($0 \le x \le 3$). Also shown in part b are the BVS values for Cu and Mn of the end-composition compounds (x = 0 and 3).

dx.doi.org/10.1021/ic401633c | *Inorg. Chem.* 2013, 52, 10610−10614

From the results of the structure refinements, we can estimate the valence states of V at the B site by a bond-valence-sum (BVS) method.[12] Although the lattice parameters increase with Mn substitution, the V−O bond distances do not change significantly and, as a result, the BVS for V is very close to +4 in all samples (Figure 4b). The V^{4+} states in the solid solutions $Ca(Cu_{3-x}Mn_x)V_4O_{12}$ are further confirmed by the V L-edge XAS spectra shown in Figure 5a. The observed spectra for the samples with $x = 0-3$ are quite similar and are essentially the same as those of V^{4+} in oxides.[13]

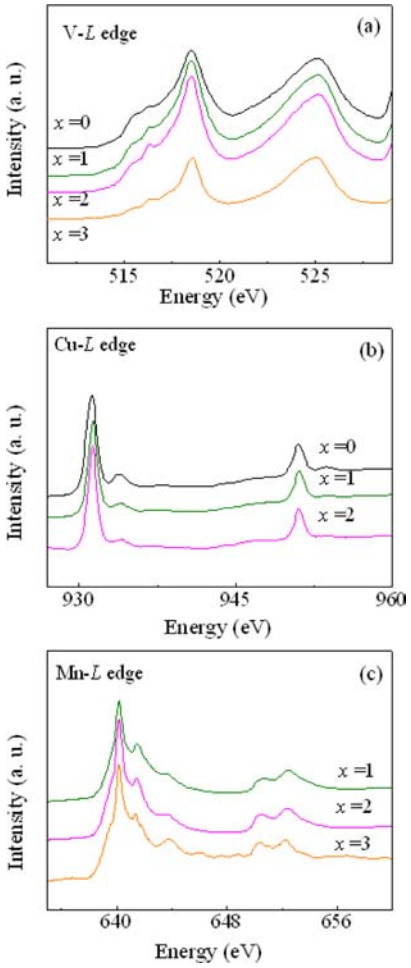

Figure 5. XAS spectra of (a) V L-edges, (b) Cu L-edges, and (c) Mn L-edges of $Ca(Cu_{3-x}Mn_x)V_4O_{12}$.

The valence states of Cu and Mn were also investigated by XAS measurements. As shown in Figure 5b,c, the observed Cu L-edge spectra, which originate from Cu 2p to 3d excitation, are quite similar to those of Cu^{2+} with d^9 electron configuration and square-planar oxygen coordination, although the peaks due to a screening effect by the conduction electrons are rather enhanced in the metallic $CaCu_3V_4O_{12}$ ($x = 0$).[14,15] The Mn L-edge spectra shapes are also very similar to the typical one of Mn^{2+},[16] and the observed spectra for the samples with $x = 1-3$ show no significant difference, indicating that the valence state of Mn in the compounds is very close to that of Mn^{2+}. Therefore, it can be concluded that for all of the solid-solution samples the basic valence states of Mn and Cu are +2, while that of V is +4. Neither Cu^{3+} nor Mn^{3+} appears to be stabilized in the present $Ca(Cu_{3-x}Mn_x)V_4O_{12}$ solid solutions. This is in sharp contrast to the Cu^{2+} substitution for Mn^{3+} at the A′ site in $A(Mn_{3-x}Cu_x)Mn_4O_{12}$ (A = Ca, Tb, Tm).[17]

Figure 6 shows the temperature dependences of the magnetic susceptibility χ and the inverse susceptibility $1/\chi$ measured at

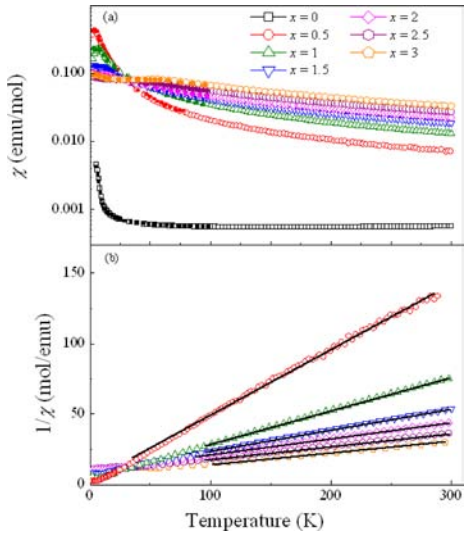

Figure 6. Temperature dependence of (a) susceptibility χ and (b) inverse susceptibility $1/\chi$ of $Ca(Cu_{3-x}Mn_x)V_4O_{12}$. Also shown by the lines in part b are the results of the Curie−Weiss fits.

1000 Oe from 2 to 300 K. As reported in a previous paper, $CaCu_3V_4O_{12}$ shows a temperature-independent Pauli-paramagnetic nature, although an increase in the susceptibility probably due to some impurity spins is observed at low temperatures. Importantly, when the Mn ions are introduced into the A′ site, Curie−Weiss-like paramagnetic behaviors appear in the solid solutions of $Ca(Cu_{3-x}Mn_x)V_4O_{12}$ ($0 < x \leq 3$). From the Curie−Weiss fits of $\chi = C/(T - \theta)$ to the paramagnetic susceptibility ($0 < x \leq 3$) at high temperature (>100 K), it is found that the Curie constants increase with increasing Mn substitution. Not unlike what is seen with $CaMn_3V_4O_{12}$ ($x = 3$), the obtained Curie constants are comparable to those expected from the Mn^{2+} spins (Figure 7). The results suggest that the Curie−Weiss paramagnetic properties of $Ca(Cu_{3-x}Mn_x)V_4O_{12}$ ($0 < x \leq 3$) originate only from the spins of the A′-site Mn. The negative Weiss constants suggest that the magnetic interaction between the Mn spins at the A′ site is antiferromagnetic and that the interaction

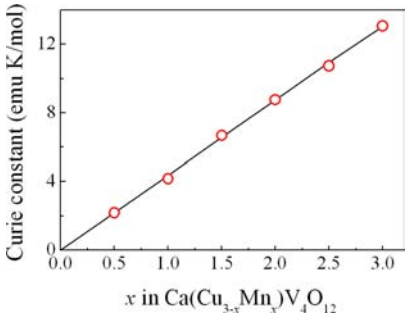

Figure 7. Curie constants of $Ca(Cu_{3-x}Mn_x)V_4O_{12}$ ($0 < x \leq 3$) obtained from the Curie−Weiss fits of the magnetic susceptibility data. The solid line shows the change of the Curie constant expected from the contribution of Mn^{2+} spins of nominal $Ca(Cu_{3-x}Mn_x)V_4O_{12}$.

dx.doi.org/10.1021/ic401633c | Inorg. Chem. 2013, 52, 10610−10614

becomes stronger with increasing Mn substitution. Although $CaMn_3V_4O_{12}$ with full Mn occupation at the A′ site shows a clear antiferromagnetic transition at 54 K, spin-glass-like behaviors, which are indicated by the difference in FC and ZFC susceptibility, are observed for the samples with $0 < x < 3$ (Figure 8). Random distribution of the Cu ions at the A′ site disturbs the long-range antiferromagnetic ordering of the Mn^{2+} spins.

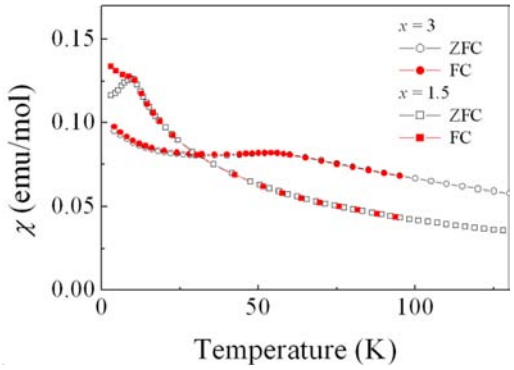

Figure 8. Temperature dependence of FC and ZFC magnetic susceptibility of $Ca(Cu_{3-x}Mn_x)V_4O_{12}$ with x = 1.5 and 3.0 at low temperatures.

Figure 9 shows the temperature dependences of resistivity from 2 to 300 K for $Ca(Cu_{3-x}Mn_x)V_4O_{12}$ ($0 \le x \le 3$). We note

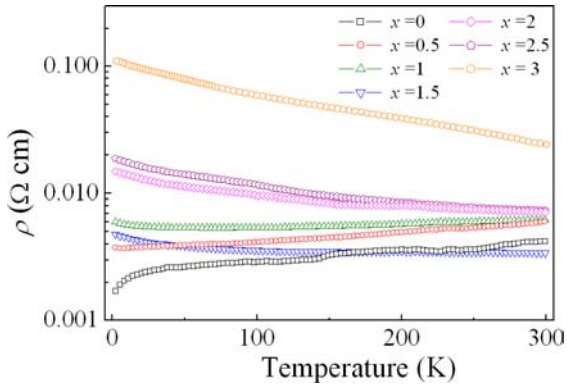

Figure 9. Temperature dependence of resistivities of $Ca(Cu_{3-x}Mn_x)V_4O_{12}$.

that all of the samples have very low resistivities, whose values are 3−10 mΩ cm at room temperature. The resistivities of the samples with $0 \le x \le 1$ increase with increasing temperature, indicating typical metallic behaviors. The resistivities of the samples with $1.5 \le x \le 3$, on the other hand, slightly decrease with increasing temperature, but the behaviors are far from a typical one of semiconductors. We thus consider that the observed transport properties include a grain-boundary effect on the polycrystalline samples and that the intrinsic transport behaviors of $Ca(Cu_{3-x}Mn_x)V_4O_{12}$ are metallic.

As we discussed in previous papers on the end-composition samples $CaCu_3V_4O_{12}$ ($x = 0$) and $CaMn_3V_4O_{12}$ ($x = 3$),[9,10] the electrons of the B-site V ions appear to be delocalized and contribute to the conductive behaviors. The electrons of the A′-site Cu ions are also delocalized, whereas those of the Mn ions at the A′ site appear to be localized, producing the local magnetic moments. Such behaviors are well explained by the characteristic electronic structures of the compounds. In $CaCu_3V_4O_{12}$, as reported in ref 9, bands originating from both the A′-site Cu and the B-site V cross the Fermi level. Finite densities of states (DOS) for Cu and V at the Fermi level are clearly seen in Figure 10a. Interestingly, for $CaCu_3V_4O_{12}$,

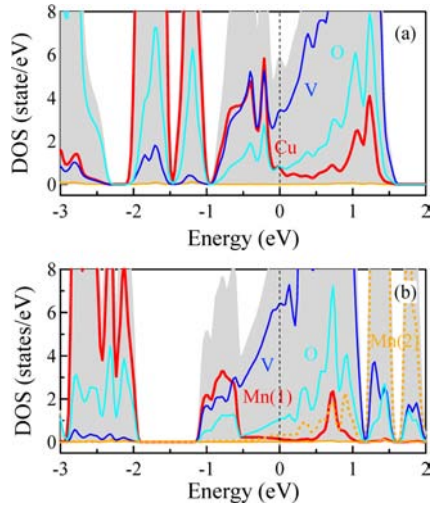

Figure 10. Calculated total (shaded region) and partial DOS for (a) paramagnetic $CaCu_3V_4O_{12}$ and (b) antiferromagnetic $CaMn_3V_4O_{12}$ (up-spin DOS only).

this paramagnetic state is more stable than an antiferromagnetic state, where the A′-site Cu spins couple antiferromagnetically. When we calculated the electronic structure with a spin-polarized initial electron configuration, the calculation converged to a state close to the paramagnetic one where equal numbers of up-spin and down-spin electrons occupy both Cu and V Muffin-tin spheres. For $CaMn_3V_4O_{12}$, in contrast, an antiferromagnetic electronic structure where the A′-site Mn spin is polarized is much more stable than the paramagnetic electronic structure. In the calculation, we tentatively assumed the G-type antiferromagnetic spin structure where the nearest-neighboring A′-site Mn spins couple antiferromagnetically, similar to the spin structure in $CaCu_3Ti_4O_{12}$.[4,6] Importantly, in the calculated electronic structure, the partial DOS for Mn are nearly zero at the Fermi level (Figure 10b). The up-spin bands of the d orbitals for Mn(1) are almost fully occupied, whereas the corresponding down-spin bands are located above the Fermi level and are empty. [The down-spin bands of the d orbitals for the neighboring Mn(2) are fully occupied, and the corresponding up-spin bands are empty.] The calculated magnetic moment of the Mn(1) Muffin-tin sphere is 4.0 μ_B/Mn, which indicates that all electrons of the Mn ions are localized. The bands originating from V, on the other hand, cross the Fermi level and contribute to the metallic conductivity. This is why we believe that the observed nonmetal-like resistivity of the $CaMn_3V_4O_{12}$ sample includes the grain-boundary effect. In $Ca(Cu_{3-x}Mn_x)V_4O_{12}$ ($0 \le x \le 1$), the Cu bands also contribute to the transport property, which makes the resistivity much lower, and even the polycrystalline samples become showing metallic behavior. Therefore, the electronic structure calculations well reproduce the experimentally observed results, where the A′-site Mn is spin-polarized and localized whereas the A′-site Cu and B-site V are delocalized. Such characteristic features of the electronic structures were evident even in the solid solution.

dx.doi.org/10.1021/ic401633c | Inorg. Chem. 2013, 52, 10610−10614

CONCLUSIONS

We made solid solutions of Pauli-paramagnetic $CaCu_3V_4O_{12}$ and antiferromagnetic $CaMn_3V_4O_{12}$, $Ca(Cu_{3-x}Mn_x)V_4O_{12}$ ($0 \leq x \leq 3$), and investigated their crystal structures, valence states of transitional-metal ions, and magnetic and transport properties. All samples crystallized in the A-site-ordered perovskite structure, and their lattice parameters changed according to Vegard's law. The results of BVS analysis and XAS suggest that the valence states of Cu and Mn at the A′ site are close to +2, whereas the valence state of V at the B site is +4 for the entire range of solid solutions. The electrons of Mn^{2+} are localized and produce $S = {}^5/_2$ magnetic moments, whereas those for Cu^{2+} are delocalized. The magnetic interaction between the Mn^{2+} spins is antiferromagnetic, and the random distribution of nonmagnetic Cu ions in the Mn spin sublattice of the A′ site results in glass-like behavior. The electrons of V, on the other hand, are delocalized and contribute to the metallic transport properties. Such characteristic features of the localized electrons of the A′-site Mn and the delocalized electrons of the A′-site Cu and B-site V are consistent with the results of electronic structure calculations, in which the bands of antiferromagnetic Mn have a spin-asymmetric gap, while those of Cu and V cross the Fermi level.

ASSOCIATED CONTENT

Supporting Information

Refined structural parameters and selected bond lengths and angles of $Ca(Cu_{3-x}Mn_x)V_4O_{12}$. This material is available free of charge via the Internet at http://pubs.acs.org.

AUTHOR INFORMATION

Corresponding Author

*E-mail: shimak@scl.kyoto-u.ac.jp. Phone: +81-774-383110. Fax: +81-774-383118.

Present Address

‡Center for Condensed Matter Science (CCMS), National Taiwan University, No. 1, Section 4, Roosevelt Road, Taipei 10617, Taiwan.

Notes

The authors declare no competing financial interest.

ACKNOWLEDGMENTS

We thank K. Osaka and I. Hirosawa for help with SXRD measurements at BL19B2 in SPring-8. The experiments in SPring-8 were performed with the approval of the Japan Synchrotron Radiation Research Institute. This work was partly supported by Grants-in-Aid for Scientific Research (Grants 19GS0207 and 22740227) and by a grant for the Joint Project of Chemical Synthesis Core Research Institutions from the Ministry of Education, Culture, Sports, Science and Technology of Japan. The work was also supported by the Japan Science and Technology Agency, CREST.

REFERENCES

(1) Homes, C. C.; Vogt, T.; Shapiro, S. M.; Wakimoto, S.; Ramirez, A. P. *Science* **2001**, *293*, 673−676.
(2) Subramanian, M. A.; Li, D.; Duan, N.; Reisner, B. A.; Sleight, A. W. *J. Solid State Chem.* **2000**, *151*, 323−325.
(3) Zeng, Z.; Greenblatt, M.; Subramanian, M. A.; Croft, M. *Phys. Rev. Lett.* **1999**, *82*, 3164−3167.
(4) Shimakawa, Y. *Inorg. Chem.* **2008**, *47*, 8562−8570.
(5) Long, Y. W.; Hayashi, N.; Azuma, M.; Muranaka, S.; Shimakawa, Y. *Nature* **2009**, *458*, 60−63.
(6) Ramirez, A. P.; Subramanian, M. A.; Gardel, M.; Blumberg, G.; Li, D.; Vogt, T.; Shapiro, S. M. *Solid State Commun.* **2000**, *115*, 217−220.
(7) Tohyama, T.; Saito, T.; Mizumaki, M.; Agui, A.; Shimakawa, Y. *Inorg. Chem.* **2010**, *49*, 2492−2495.
(8) Tohyama, T.; Senn, Mark, S.; Saito, T.; Chen, W.-T.; Tang, C. C.; Attfield, J. P.; Shimakawa, Y. *Chem. Mater.* **2013**, *25*, 178−183.
(9) Shiraki, H.; Saito, T.; Azuma, M.; Shimakawa, Y. *J. Phys. Soc. Jpn.* **2008**, *77*, 064705 (1−4).
(10) Zhang, S. B.; Saito, T.; Mizumaki, M.; Chen, W.-T.; Tohyama, T.; Shimakawa, Y. *J. Am. Chem. Soc.* **2013**, *135*, 6056−6060.
(11) Larson, A. C.; Von Dreele, R. B.*Los Alamos National Laboratory Report LAUR*; Los Alamos National Laboratory: Los Alamos, NM, 2004; pp 86−784.
(12) Brown, I. D.; Altermatt, D. *Acta Crystallogr.* **1985**, *B41*, 244−247.
(13) Pen, H. F.; Abbate, M.; Fujimori, A.; Tokura, Y.; Eisaki, H.; Uchida, S.; Sawatzky, G. A. *Phys. Rev. B* **1999**, *59*, 7422−7432.
(14) Huang, S. W.; Huang, D. J.; Okamoto, J.; Wu, W. B.; Chen, C. T.; Yeh, K. W.; Chen, C. L.; Wu, M. K.; Hsu, H. C.; Chou, F. C. *Solid State Commun.* **2008**, *147*, 234−237.
(15) Mizumaki, M.; Saito, T.; Chen, W.-T.; Yamada, I.; Attfield, J. P.; Shimakawa, Y. *Phys. Rev. B* **2011**, *84*, 094418 (1−4).
(16) Gilbert, B.; Frazer, B. H.; Belz, A.; Conrad, P. G.; Nealson, K. H.; Haskel, D.; Lang, J. C.; Srajer, G.; De Stasio, G. *J. Phys. Chem. A* **2003**, *107*, 2839−2847.
(17) Troyanchuk, I. O.; Lobanovsky, L. S.; Kasper, N. V.; Hervieu, M.; Maignan, A.; Michel, C. *Phys. Rev. B* **1998**, *58*, 14903−14907.